## Site-Resolved Near-Surface Cation Diffusion in Magnetite

Steffen Tober®, <sup>1,2,3,4,\*</sup> Jan-Christian Schober®, <sup>1,2</sup> Marcus Creutzburg®, <sup>1</sup> Esko Erik Beck, <sup>1,2</sup> Guilherme Dalla Lana Semione®, <sup>1,2</sup> Simon Chung®, <sup>1</sup> Leon Jacobse®, <sup>1</sup> Björn Arndt, <sup>1</sup> Alina Vlad®, <sup>5</sup> René Steinbrügge®, <sup>6</sup> Hans-Christian Wille®, <sup>6</sup> Ilya Sergueev®, <sup>6</sup> Heshmat Noei®, <sup>1</sup> Kai Schlage®, <sup>6</sup> Olaf Leupold®, <sup>6</sup> Vedran Vonk®, <sup>1,†</sup> and Andreas Stierle®<sup>1,2,‡</sup>

<sup>1</sup>Centre for X-ray and Nano Science CXNS, Deutsches Elektronen-Synchrotron DESY, Notkestr. 85, 22607 Hamburg, Germany

<sup>2</sup>Department of Physics, University of Hamburg, Jungiusstr. 11, 20355 Hamburg, Germany

<sup>3</sup>Jülich Centre of Neutron Science (JCNS-2), Forschungszentrum Jülich, Wilhelm-Johnen-Str., 52428 Jülich, Germany

<sup>4</sup>Institute for a Sustainable Hydrogen Economy (INW), Forschungszentrum Jülich, Marie-Curie-Str. 5, 52428 Jülich, Germany

<sup>5</sup>Synchrotron SOLEIL, L'Orme des Merisiers, 91190 Saint-Aubin, France

<sup>6</sup>Deutsches Elektronen-Synchrotron DESY, Notkestr. 85, 22607 Hamburg, Germany

(Received 13 March 2024; accepted 28 March 2025; published 13 June 2025)

In situ nuclear forward scattering shows a thermally induced cation exchange between a  $^{57}\text{Fe}_3\text{O}_4$  thin-film and a Fe $_3\text{O}_4$  (001) substrate predominantly in the octahedral sublattice for a temperature range between 470 and 710 K. The overall activation barrier in this temperature range is found to be  $19 \pm 32$  kJ/mol, which is significantly lower than expected from extrapolating a bulk diffusion model. This observation can be attributed to the large out-of-equilibrium cation deficit as determined by surface x-ray diffraction. Despite the relatively low hopping barrier, the diffusion constant is about 5 orders of magnitude lower than expected for magnetite having an equilibrium cation stoichiometry. The results are relevant for applications relying on the near-surface structure and stoichiometry of magnetite, and we argue that the correlation between cation diffusion and stoichiometry may play a role for a wider range of oxide materials.

DOI: 10.1103/PhysRevLett.134.236203

The properties of magnetite (Fe<sub>3</sub>O<sub>4</sub>) nanostructures, intensively studied for applications in new materials, medicine, and catalysis, are strongly influenced by the defect structure and stability of their near-surface region [1–7]. Near-surface cation transport is involved in restructuring and phase transformations of nanoparticles [8,9] and surfaces such as oxidative regrowth processes [10] or the formation and lifting of the subsurface cation vacancy (SCV) reconstruction on Fe<sub>3</sub>O<sub>4</sub> (100) surfaces [11–13]. As a mixed valence compound with a relatively variable stoichiometry, Fe<sub>3</sub>O<sub>4</sub> can easily incorporate adatoms at the surface, making it a promising support material in single atom catalysts [14–17]. Their performance, in turn, depends crucially on their near-surface cation dynamics [18,19]. Considering the rich chemistry of cubic iron oxides, cation transport in  $Fe_{3-\delta}O_4$  related to the temperature- and pressure-dependent nonstoichiometry  $\delta$  is

\*Contact author: steffen.tober@desy.de †Contact author: vedran.vonk@desy.de ‡Contact author: andreas.stierle@desy.de

Published by the American Physical Society under the terms of the Creative Commons Attribution 4.0 International license. Further distribution of this work must maintain attribution to the author(s) and the published article's title, journal citation, and DOI. described by the so-called point defect model, based on bulk diffusion models and data from single- and polycrystalline samples [20–23]. Tuning the shape and chemical properties of Fe<sub>3</sub>O<sub>4</sub>-based materials, nanoparticles, catalysts, and devices therefore requires additional knowledge about the near-surface defect structure and cation migration as well as its relation to structural disorder and chemical gradients [24–26]. Fe<sub>3</sub>O<sub>4</sub> has an inverse spinel structure with a face-centered cubic oxygen sublattice. As shown in Fig. 1(a),  $\frac{1}{8}$  of the 64 tetrahedral (tet) sites are occupied by  $Fe^{3+}$ , and  $\frac{1}{4}$  each of the 32 octahedral (oct) lattice sites are filled by Fe<sup>3+</sup> and Fe<sup>2+</sup>. They exhibit a ferrimagnetic spin order between the Verwey transition at 125 K and the Néel temperature at 870 K [27,28]. Owing to fast electron hopping in stoichiometric Fe<sub>3</sub>O<sub>4</sub>,  $(Fe^{3+} + e^{-} \rightleftharpoons Fe^{2+})$  the oct cations correspond on average to Fe<sup>2.5+</sup> [29,30]. Nonstoichiometric (Fe<sub>3- $\delta$ </sub>O<sub>4</sub>), further oxidized maghemite (γ-Fe<sub>2</sub>O<sub>3</sub>), or more reduced wüstite (FeO) are formed without relevant changes in the rigid oxygen sublattice (see the Supplemental Material, Fig. S1 [31]) [29]. In the following, we present a sublatticeresolved observation of near-surface cation transport at the interface of <sup>57</sup>Fe<sub>3</sub>O<sub>4</sub> thin films and a Fe<sub>3</sub>O<sub>4</sub> substrate by nuclear forward scattering of synchrotron radiation (NFS), taking into account its near-surface defect structure

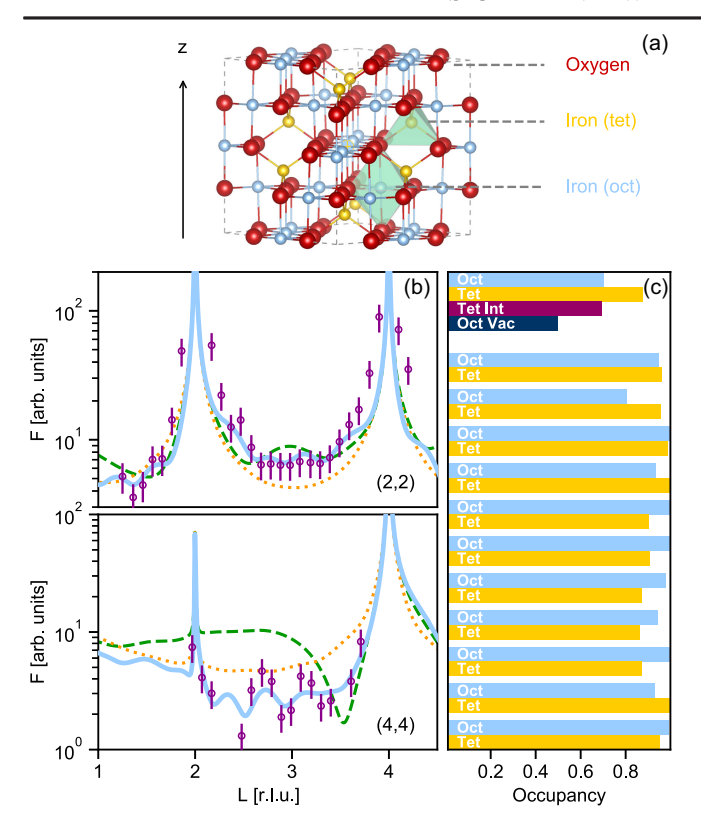


FIG. 1. (a) The bulk unit cell of  $Fe_3O_4$ . Oxygen is shown in red,  $Fe_{tet}$  in yellow,  $Fe_{oct}$  in light blue. (b) The (2,2) and (4,4) CTRs (purple symbols) of the 52 Å<sup>nat</sup> $Fe_3O_4$  thin film on <sup>nat</sup> $Fe_3O_4$  (001). The fit (light blue solid line) is compared with simulations for a bulk truncated (yellow dotted line) and the SCV reconstructed surface (green dashed line). (c) Layer-resolved cation occupancy profile for iron tet (yellow) and oct (light blue) in the topmost three unit cells of the thin film with the tet interstitial and oct vacancies of the SCV surface.

determined by *in situ* surface x-ray diffraction (SXRD) of a similar Fe<sub>3</sub>O<sub>4</sub> thin film.

Natural (001) oriented  $^{nat}Fe_3O_4$  single crystal substrates (10  $\times$  10 mm, miscut < 0.1°) were prepared by subsequent cycles of  $Ar^+$  sputtering at  $5\times 10^{-6}$  mbar/1 kV, followed by annealing at 930 K in ultrahigh vacuum (UHV). The last annealing step was carried out in  $1\times 10^{-6}$  mbar  $O_2$  to form the ( $\sqrt{2}\times\sqrt{2}$ ) R45° pattern of the SCV reconstructed surface [12]. Thin films were homoepitaxially grown by reactive molecular beam epitaxy (MBE) at a substrate temperature of 420 K in  $8\times 10^{-7}$  mbar  $O_2$  (99.999% purity) with a growth rate of 0.015 Å/s.

To label the cations of the near-surface region, a 70 Å<sup>57</sup>Fe<sub>3</sub>O<sub>4</sub> thin film on <sup>nat</sup>Fe<sub>3</sub>O<sub>4</sub> was grown from a <sup>57</sup>Fe rod (99.99% chemical purity, enriched to 95% <sup>57</sup>Fe) and precharacterized after transfer through air by x-ray photoelectron spectroscopy (XPS) at DESY NanoLab [38].

The near-surface defect structure of homoepitaxial magnetite thin films was studied at the SixS beamline of SOLEIL [39]. A 52 Å  $^{nat}$ Fe $_3O_4$  on  $^{nat}$ Fe $_3O_4$  (001) sample

was prepared. Eight independent crystal truncation rods (CTR) and their symmetry equivalents were measured in situ. The CTRs were fitted by ROD from the ANAROD package to a model consisting of three unit cells with a lattice constant of a = 8.394 Å based on the SCV reconstructed magnetite surface with the structural motif of an interstitial tet cation in the first atomic layer and two oct vacancies in the layer below (see the Supplemental Material Fig. S2 [31]) [12,27,40]. Comparison of the data with simulated CTRs of bulk truncated and SCV surfaces in Fig. 1(b) suggests that the SCV reconstruction is present, but coexists with regions without long-range SCV order. A similar observation was made for surfaces annealed above a critical temperature of 745 K [13]. The SCV reconstruction is also lifted by formation of an iron rich octahedral pair surface (partially) after deposition of a few monolayers of iron on Fe<sub>3</sub>O<sub>4</sub> [17]. At temperatures of 523 K as used herein, iron diffusion from the surface into the crystal was observed [17]. Low-energy electron diffraction (LEED), probing a smaller surface area, confirmed the (partial) presence of the SCV reconstruction for a comparable 50 Å thin film in Fig. S4, in the Supplemental Material [31]. Only minor atom displacements compared to the model were observed, but a substantial cation deficit of up to 10% in the oct and tet sublattices was found, as shown in Fig. 1(c); similar findings were reported for Fe<sub>3</sub>O<sub>4</sub> thin films on MgO and (001)-oriented spinel (MgAl<sub>2</sub>O<sub>4</sub>) surfaces [41–43]. The approximate sum formula in the first three unit cells therefore is Fe<sub>2.7</sub>O<sub>4</sub> [42]. X-ray reflectivity (XRR) suggests a cation deficit for the full depth of the thin film (see Fig. S3 [31]). The Fe<sub>3</sub>O<sub>4</sub>-like structure was formed due to kinetic stabilization by the substrate, although thermodynamically unfavorable under the given conditions [44,45]. A more detailed description of the homoepitaxial growth of Fe<sub>3</sub>O<sub>4</sub> will be given elsewhere.

Cation migration between the 70 Å  $^{57}\text{Fe}_3\text{O}_4$  thin film and its  $^{\text{nat}}\text{Fe}_3\text{O}_4$  (001) substrate was monitored by NFS at the P01 beamline of PETRAIII, operated in a 40-bunch mode with a bunch separation of 192 ns. The photon energy was adjusted to the  $^{57}\text{Fe}$  Mössbauer resonance at 14.413 keV by a high resolution silicon monochromator with an energy resolution of  $\sim$ 1 meV [46]. Resonantly and nonresonantly scattered photons were detected by four stacked avalanche photo diodes. *In situ* annealing experiments were done in a UHV chamber with a base pressure of  $1 \times 10^{-9}$  mbar, equipped with a precalibrated ceramic heater and Fe-free Be windows.

NFS combines the spatial sensitivity of x-ray scattering methods due to the temporal and spatial coherence of the synchrotron beam with the isotope and chemical sensitivity of Mössbauer spectroscopy probing the hyperfine interactions of <sup>57</sup>Fe. Time spectra (TS), the temporal evolution of the signal due to an interference of the decays of excited nuclear states, provide information about the composition of the sample. They were measured at incidence angles of 0.13° and 0.19° (below and above the critical angle

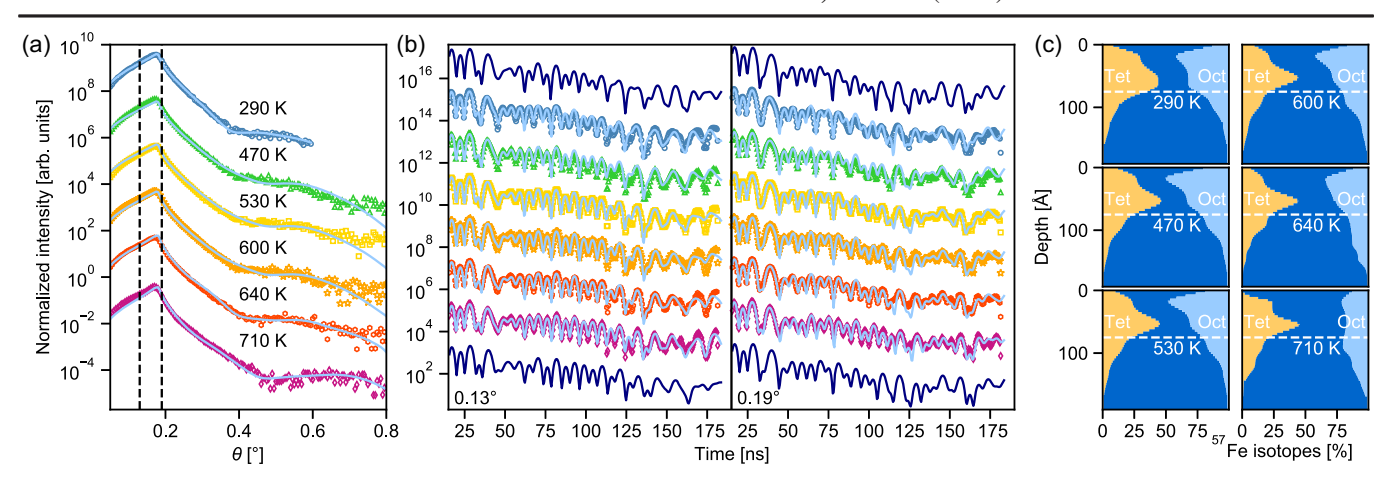


FIG. 2. (a) NRR curves (symbols) and corresponding fits (light blue solid lines) of a 70 Å $^{57}$ Fe<sub>3</sub>O<sub>4</sub> thin film on Fe<sub>3</sub>O<sub>4</sub>. Time spectra were measured at the angles indicated by dashed lines. For clarity, the curves are plotted with a *y* offset. (b) Time spectra (symbols) at incidence angles of 0.13° and 0.19° measured after the heating steps and the corresponding fits (solid lines). Simulations with a 1:2 ratio of Fe<sub>tet</sub> and Fe<sub>oct</sub> using the fit parameters obtained for the sample after growth (top) and after annealing (bottom) at 710 K are shown as dark blue solid lines for comparison. (c) Depth-dependent site-selective <sup>57</sup>Fe distribution after the respective annealing step obtained from NFS. The <sup>57</sup>Fe<sub>tet</sub> is shown in yellow, <sup>57</sup>Fe<sub>oct</sub> in light blue. The remaining iron sites are assumed to be occupied by nonresonant isotopes shown in dark blue; 100% Fe refers to the density at the respective depth.

 $\alpha_{\rm c}=0.175^{\circ}$ ), thus varying the probing depth around the film/substrate interface. Nuclear resonant reflectivity (NRR) probes the isotope depth profile on the subnanometer scale and is therefore sensitive to subtle changes, as expected for near-surface cation transport at modest temperatures [24,47]. The sample was annealed stepwise respectively at 470, 530, 600, 640, and 710 K for 15 min, reaching pressures in the  $10^{-7}$  mbar range due to residual molecules desorbing from the sample environment. NRR and TS were collected after each annealing step at room temperature in UHV. Simultaneously measured XRR from nonresonant photons enabled disentangling the isotope depth-distribution determined from NRR and the electron density. For the as-grown sample, XRR showed a minor reduction of the electron density at the surface, maybe due to surface oxidation. This is in agreement with the cation deficit observed by SXRD and the slightly increased amount of Fe<sup>3+</sup> observed by XPS (see the Supplemental Material, Figs. S5 and S6 [31]).

During annealing, the featureless XRR in Fig. S6 remained nearly unchanged whereas the single damped oscillation of the NRR in Fig. 2(a) resulting from the isotope contrast shifted toward higher angles. The cation deficit in the near-suface region seemingly was maintained despite the cation exchange across the thin-film/substrate interface. Only subtle changes were observed in the TS in Fig. 2(b).

The <sup>57</sup>Fe depth distribution shown in Fig. 2(c) was derived form a joint fit of NRR and TS with REFTIM, based on the remodeled electron density profiles obtained from XRR fitted with GenX [48–50]. The sample was modeled by four slabs of variable thickness on the infinite <sup>nat</sup>Fe<sub>3</sub>O<sub>4</sub> substrate. From the sample surface, the slabs I

and II represent the <sup>57</sup>Fe<sub>3</sub>O<sub>4</sub> thin film, III the thin-film/ single crystal interface, and IV the top part of the natFe<sub>3</sub>O<sub>4</sub> single crystal. To account for the progressing diffusion of <sup>57</sup>Fe into the single crystal, a fifth slab was added below for the annealing steps at 640 and 710 K. Two multiplets are associated with the  $Fe^{3+}$  and on average  $Fe^{2.5+}$  cations of the tet and oct sublattices in Fe<sub>3</sub>O<sub>4</sub>. For them, hyperfine interactions, slab thicknesses, and roughnesses were fitted separately. The deviating isomer shifts and hyperfine fields of 48.9 T and 45.9 T for tet and oct cause two characteristic, interfering beating patterns in the TS. Fitting the TS thereby allows one to distinguish the lattice sites. A third multiplet with maghemitelike hyperfine interactions was allowed, but had no significant impact, suggesting a formation of maghemite only below the detection limit. All fit parameters and reference values of the hyperfine interactions are given in the Supplemental Material, Tables SI-SIV, densitiy normalized profiles in Fig. S7 [31]. Isomer shift, hyperfine fields, and their distributions stayed close to the values for Fe<sub>3</sub>O<sub>4</sub> within the typical experimental error, showing that no major chemical transformation was caused by the annealing [51].

Initially, about 75% of the cation sites in slabs I and II were populated by <sup>57</sup>Fe. Remaining cation sites were occupied by nonresonant isotopes, in the following termed as <sup>non</sup>Fe. The <sup>57</sup>Fe concentration in slabs III–V gradually increased compared to natural Fe<sub>3</sub>O<sub>4</sub>, because deposited <sup>57</sup>Fe and <sup>non</sup>Fe ions from the substrate likely intermixed during deposition [52]. Annealing at 470 K decreased the <sup>57</sup>Fe<sub>oct</sub> concentration in slab III as well as the overall concentration of <sup>57</sup>Fe in slabs I and II, indicating <sup>57</sup>Fe transport toward the bulk. This trend continued for the following annealing steps.

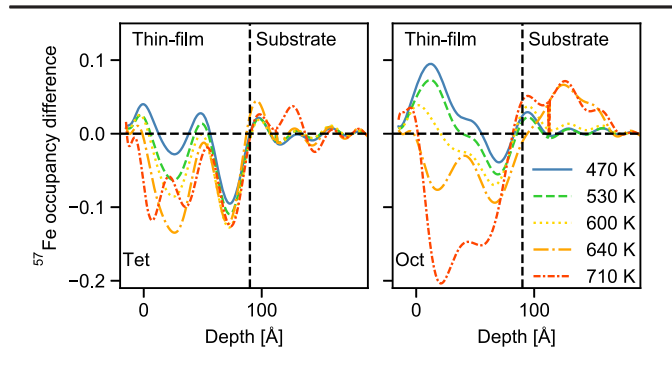


FIG. 3. Occupancy difference in the tet and oct sublattice between the initial <sup>57</sup>Fe distribution and after annealing at the respective temperature. The vertical line marks the center of thin-film/substrate interface at a depth of a 90 Å.

The apparent <sup>57</sup>Fe<sub>tet</sub>/<sup>57</sup>Fe<sub>oct</sub> ratio in the first two slabs was close to 1:1, with the amount of <sup>57</sup>Fe<sub>tet</sub> exceeding 33% of the total iron in slab II. This partly is a result of siteselective cation transport during deposition. As the formation of  ${}^{57}\text{Fe}^{3+}_{\text{tet}}$  interstitials is highly unlikely in the given chemical environment, the excess of <sup>57</sup>Fe<sub>tet</sub> beyond the structural limits of Fe<sub>3</sub>O<sub>4</sub> in slab II is attributed to charge trapping effects observed in earlier Mössbauer spectroscopy studies of understoichiometric  $Fe_{3-\delta}O_4$  thin films [53]. Electron hopping in the oct sublattice is faster than the lifetime of the nuclear excitation. NFS therefore probes the convoluted hyperfine interactions of <sup>57</sup>Fe<sub>oct</sub><sup>3+</sup> and <sup>57</sup>Fe<sub>oct</sub><sup>2+</sup>, termed <sup>57</sup>Fe<sup>2.5+</sup><sub>oct</sub>. These hyperfine interactions are clearly distinguishable from those of <sup>57</sup>Fe<sub>tet</sub> [30,53]. In understoichiometric Fe<sub>3-\delta</sub>O<sub>4</sub>, five Fe<sub>oct</sub> per vacancy are trapped in a  $Fe_{oct}^{3+}$  state to compensate for the nominal -2.5 charge of the vacancies in the oct sublattice. Thus, they do not participate in the electron hopping. The hyperfine interactions of Fe<sub>oct</sub> and Fe<sub>tet</sub> are strongly overlapping and therefore barely distinguishable. The amount of <sup>57</sup>Fe<sub>tet</sub><sup>3+</sup> is overestimated, and that of <sup>57</sup>Fe<sub>oct</sub> is underestimated by the fit [53]. The apparent surplus of Fe<sub>tet</sub> estimated from NFS largely agrees with the Fe<sub>oct</sub> deficit of 10% suggested by SXRD and also with earlier observations by x-ray resonant magnetic reflectivity and Mössbauer spectroscopy [30,41].

To illustrate the cation transport process, the tet and oct cation distribution profiles after the respective annealing steps were subtracted from the initial state and plotted in Fig. 3. Thermally induced cation transport across the thin-film/substrate interface mainly takes place in the oct sublattice, visible by the persistently decreasing <sup>57</sup>Fe concentration in slab II and increasing <sup>57</sup>Fe concentration in slabs III–V from 470 to 710 K. Significant cation exchange in the tet lattice seems to start only at 640 K.

Two seemingly counterintuitive observations may result from oxidation and reduction processes within the magnetite structure. After annealing at 470 K, the  $^{57}$ Fe<sub>tet</sub> amount decreases. This can result from a reduction of the sample

surface. Being transferred through air, the sample was slightly oxidized during the measurement at room temperature, enhancing charge trapping and causing a seemingly increased <sup>57</sup>Fe<sub>tet</sub> concentration due to the presence of <sup>57</sup>Fe<sub>oct</sub>. Vacuum annealing reduced the <sup>57</sup>Fe<sub>oct</sub>, and thus caused the seeming decrease of Fe<sub>tet</sub> and the corresponding increase of Fe<sub>oct</sub> in slab I. The back diffusion of <sup>57</sup>Fe<sub>tet</sub> to the thin-film surface at 710 K may be related to the onset of oxidative regrowth of Fe<sub>3</sub>O<sub>4</sub> reported for similar conditions [10]. This process can partly compensate for the <sup>57</sup>Fe migration into the substrate, but also leads to oxidation and charge trapping causing the increase of the <sup>57</sup>Fe<sub>tet</sub>-like hyperfine interactions.

For comparison of near-surface and bulk cation transport in  $\mathrm{Fe_3O_4}$ , diffusion coefficients were estimated by fitting diffusion profiles to the overall  $^{57}\mathrm{Fe}$  depth profiles at the thin-film/substrate interface, as shown in the Supplemental Material, Fig. S8 and Table SV [31].

Cation transport in bulk Fe<sub>3</sub>O<sub>4</sub> in dependence of temperature T and oxygen activity  $a_{O_2}$  is described by the point defect model by Dieckmann and Schmalzried [20,21,54]. Under reducing conditions, cations migrate via an intersticialcy process in the tet sublattice, under oxidizing conditions via a vacancy mechanism in the oct sublattice, mainly depending on the vacancy formation that saturates under oxidizing conditions outside the thermodynamic stability range of Fe<sub>3</sub>O<sub>4</sub> [20-22,54]. Further details are given in the Supplemental Material [31]. The measured near-surface diffusion coefficients are up to 5 orders of magnitude smaller compared to the point defect model, but in agreement with previously reported near-surface diffusion coefficients determined in a similar temperature range by neutron reflectivity, and larger than diffusion coefficients expected under fully stoichiometric conditions. The latter are considered as the lower limit for cation transport in magnetite [52,55]. Near-surface diffusion coefficients are plotted in Fig. 4 together with the point defect model for similar conditions and for perfectly stoichiometric magnetite without formation of additional defects [21]. Obviously, our kinetically stabilized, cation deficient sample, as proved by SXRD and NFS, is not described accurately by the point defect model, even in view of its limited reliability at low temperatures [56]. Considering the nearly linear relation of temperature and diffusion coefficients in the small probed temperature range and the observation of cation transport mainly in the oct sublattice, the vacancy part of the point defect model can be reverted to the basic diffusion equation in its Arrhenius form in Eq. (1) [57]:

$$D = D^0 e^{\frac{-E_a}{RT}} = \gamma f d^2 x_{\text{vac}} \nu e^{\frac{-\Delta S_m}{RT}} e^{\frac{\Delta H_v}{RT}} e^{\frac{\Delta H_m}{RT}}$$
(1)

From the Arrhenius plot in Fig. 4  $E_{\rm A}=19\pm32$  kJ/mol and  $D^0=3.5\times10^{-20\pm3}$  m²/s were estimated. Despite the considerable error, they are clearly smaller than the bulk values of  $E_{\rm A}=86$  kJ/mol and  $D^0=4.43\times10^{-15}$  m²/s

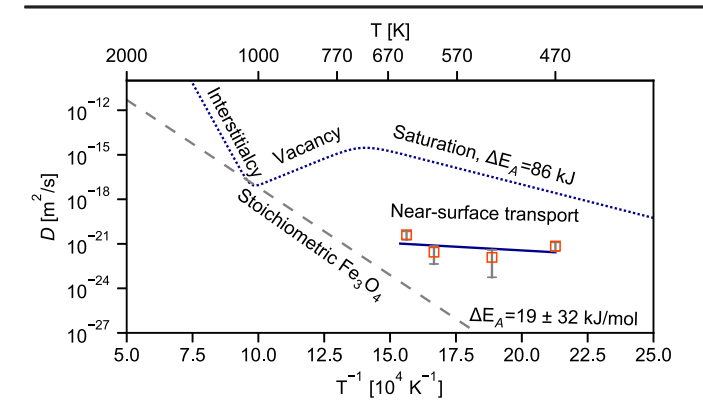


FIG. 4. The diffusion coefficients estimated from the  $^{57}$ Fe distribution profiles (red open squares) compared to the point defect model proposed in [20,54] (blue dotted line) at  $a_{\rm O_2} = 1 \times 10^{-12}$  mbar and the simple diffusion equation-based model from Eq. (1) (blue solid line). The temperature dependent diffusion coefficients in stoichiometric Fe<sub>3</sub>O<sub>4</sub> are indicated by the gray dashed line [55].

from the point defect model [54]. The decrease of both  $D^0$  and  $E_A$  is in good agreement with the more general correlation of  $E_A$  and  $D^0$  described by Faupel *et al.* for crystalline but also amorphous materials and the data for metallic glasses found by Gupta *et al.* [24,25,58].

While the precise mechanistic distinction between near-surface and bulk transport remains unclear, splitting Eq. (1) into its components allows one to identify influences reducing  $D^0$  and  $E_{\rm A}$ , as previously demonstrated by Stelter *et al.* [59].

Depending on the crystal geometry, the lattice specific geometric factor  $\gamma$  and the jump distance d are not expected to change significantly in the near-surface region. The correlation factor f, 0 for random and 1 for fully correlated jumps, cannot cause a difference in  $D^0$  of several orders of magnitude. Instead the increased vacancy concentration  $x_{\text{vac}}$ in the near-surface region, leading to electronic changes visible as charge trapping in NFS and structural distortions in SXRD, may have decreased  $E_A$ , consisting of the entropy of motion  $\Delta S_{\rm m}$ , as well as the vacancy formation and motion enthalpies  $\Delta H_{\rm v}$  and  $\Delta H_{\rm m}$ , by reduction of  $\Delta H_{\rm v}$ . Charge trapping also may have significantly reduced the attempt frequency  $\nu$  that commonly is on the order of  $10^{13}$  1/s, causing the reduction of  $D^0$ . This is well in line with the vacancy diffusion mechanism suggested by Muhich et al. During migration, an Fe<sup>3+</sup> cation neighboring a vacancy is partly reduced requiring charge redistribution in the oct lattice that is hindered by charge trapping in understoichiometric Fe<sub>3</sub>O<sub>4</sub> [23]. This may also explain the, albeit to a lower extent, experimentally observed slower cation migration in understoichiometric bulk Fe<sub>3</sub>O<sub>4</sub> [60]. In the near-surface region, oxidative regrowth at the surface, as observed by Nie et al., may have further counteracted the cation exchange between bulk and tracer film, without affecting the actual diffusion mechanism [10].

In summary, we used a <sup>57</sup>Fe<sub>3</sub>O<sub>4</sub> tracer film to probe temperature induced near-surface cation transport by NFS and evaluated the results with respect to the defect structure of homoepitaxially grown Fe<sub>3</sub>O<sub>4</sub>, determined by SXRD. Site selective monitoring of composition and <sup>57</sup>Fe depth distribution indicated cation transport starting at 470 K from the thin film to the substrate, mainly via the octahedral sublattice in agreement with the vacancy mechanism in the point defect model, although with considerably smaller diffusion coefficients. Arguably, this can be attributed to the high near-surface defect concentrations affecting the vacancy transport mechanism. The proposed interplay of near-surface defect structure and cation transport is particularly relevant for thin-film preparation, nanostructured catalysts, and nanoparticles with their high surface-tovolume ratio. As the probed MBE-grown thin film, these structures are to a large extent kinetically stabilized [2,9]. The slow cation migration may be a reason for the formation of Fe<sub>3</sub>O<sub>4</sub> even under thermodynamically unfavorable conditions in heteroepitaxial thin-film growth [45,61] or, in general, kinetically hinder the transformation of metastable perovskite phases [62]. Slowing down cation transport by defect engineering helps to prevent the structural degradation of nanoparticles in medical applications, as well as to stabilize catalytic sites in heterogeneous catalysts improving their performance.

Acknowledgments—We acknowledge DESY (Hamburg, Germany), a member of the Helmholtz Association HGF, for the provision of experimental facilities for NFS at beamline P01 as well as SOLEIL for provision of synchrotron radiation facilities for SXRD and A. Resta, B. Voisin, and A. Coati for assistance in using the SixS beamline. We thank Marina A. Andreeva for advice with the usage of REFTIM. Funding by the Deutsche Forschungsge meinschaft (DFG, German Research Foundation)—Projektnummer 192346071—SFB 986 is acknowledged.

Data availability—The data that support the findings of this article are not publicly available. The data are available from the authors upon reasonable request.

<sup>[1]</sup> O. T. Bruns, H. Ittrich, K. Peldschus, M. G. Kaul, U. I. Tromsdorf, J. Lauterwasser, M. S. Nikolic, B. Mollwitz, M. Merkel, N. C. Bigall, S. Sapra, R. Reimer, H. Hohenberg, H. Weller, A. Eychmüller, G. Adam, U. Beisiegel, and J. Heeren, Nat. Nanotechnol. 4, 193 (2009).

<sup>[2]</sup> A. Baeza, G. Guillena, and D. J. Ramón, ChemCatChem 8, 49 (2016).

<sup>[3]</sup> K. R. P. M. Rao, F. E. Huggins, V. Mahajan, G. P. Huffman, V. U. S. Rao, B. L. Bhatt, D. B. Bukur, B. H. Davis, and R. J. O'Brien, Top. Catal. 2, 71 (1995).

<sup>[4]</sup> A. Dreyer, A. Feld, A. Kornowski, E. D. Yilmaz, H. Noei, A. Meyer, T. Krekeler, C. Jiao, A. Stierle, V. Abetz, H. Weller, and G. A. Schneider, Nat. Mater. 15, 522 (2016).

- [5] N. Nandakumaran, L. Barnsley, A. Feoktystov, S. A. Ivanov, D. L. Huber, L. S. Fruhner, V. Leffler, S. Ehlert, E. Kentzinger, A. Qdemat, T. Bhatnagar-Schöffmann, U. Rücker, M. T. Wharmby, A. Cervellino, R. E. Dunin-Borkowski, T. Brückel, and M. Feygenson, Adv. Mater. 33, 2008683 (2021).
- [6] M. Creutzburg, M. Konuk, S. Tober, S. Chung, B. Arndt, H. Noei, R. H. Meißner, and A. Stierle, Commun. Chem. 5, 134 (2022).
- [7] E. Gürsoy, G. B. Vonbun-Feldbauer, and R. H. Meißner, J. Phys. Chem. Lett. 14, 6800 (2023).
- [8] A. Feld, A. Weimer, A. Kornowski, N. Winckelmans, J.-P. Merkl, H. Kloust, R. Zierold, C. Schmidtke, T. Schotten, M. Riedner, S. Bals, and H. Weller, ACS Nano 13, 152 (2019).
- [9] T. Köhler, A. Feoktystov, O. Petracic, E. Kentzinger, T. Bhatnagar-Schöffmann, M. Feygenson, N. Nandakumaran, J. Landers, H. Wende, A. Cervellino, U. Rücker, A. Kovács, R. E. Dunin-Borkowski, and T. Brückel, Nanoscale 13, 6965 (2021).
- [10] S. Nie, E. Starodub, M. Monti, D. A. Siegel, L. Vergara, F. El Gabaly, N. C. Bartelt, J. de la Figuera, and K. F. McCarty, J. Am. Chem. Soc. 135, 10091 (2013).
- [11] R. Bliem, E. McDermott, P. Ferstl, M. Setvin, O. Gamba, J. Pavelec, M. A. Schneider, M. Schmid, U. Diebold, P. Blaha, L. Hammer, and G. S. Parkinson, Science 346, 1215 (2014).
- [12] B. Arndt, R. Bliem, O. Gamba, J. E. van der Hoeven, H. Noei, U. Diebold, G. S. Parkinson, and A. Stierle, Surf. Sci. 653, 76 (2016).
- [13] B. Arndt, B. A. J. Lechner, A. Bourgund, E. Granas, M. Creutzburg, K. Krausert, J. Hulva, G. S. Parkinson, M. Schmid, V. Vonk, F. Esch, and A. Stierle, Phys. Chem. Chem. Phys. 22, 8336 (2020).
- [14] N. Comini, J. T. Diulus, G. S. Parkinson, J. Osterwalder, and Z. Novotny, J. Phys. Chem. C 127, 19097 (2023).
- [15] R. Bliem, J. Pavelec, O. Gamba, E. McDermott, Z. Wang, S. Gerhold, M. Wagner, J. Osiecki, K. Schulte, M. Schmid, P. Blaha, U. Diebold, and G. S. Parkinson, Phys. Rev. B 92, 075440 (2015).
- [16] F. Mirabella, M. Müllner, T. Touzalin, M. Riva, Z. Jakub, F. Kraushofer, M. Schmid, M. T. M. Koper, G. S. Parkinson, and U. Diebold, Electrochim. Acta 389, 138638 (2021).
- [17] O. Gamba, M. Eder, M. Poglitsch, J. Pavelec, P. Sombut, M. Meier, U. Diebold, M. Schmid, and G. S. Parkinson, Mater. Res. Express 10, 116517 (2023).
- [18] J. Hulva, M. Meier, R. Bliem, Z. Jakub, F. Kraushofer, M. Schmid, U. Diebold, C. Franchini, and G. S. Parkinson, Science 371, 375 (2021).
- [19] E. Bianchetti, D. Perilli, and C. Di Valentin, ACS Catal. **13**, 4811 (2023).
- [20] R. Dieckmann and H. Schmalzried, Ber. Bunsengesellschaft Phys. Chem. 81, 344 (1977).
- [21] R. Dieckmann and H. Schmalzried, Ber. Bunsengesellschaft Phys. Chem. 90, 564 (1986).
- [22] K. D. Becker, V. V. Wurmb, and F. J. Litterst, J. Phys. Chem. Solids 54, 923 (1993).
- [23] C. L. Muhich, V. J. Aston, R. M. Trottier, A. W. Weimer, and C. B. Musgrave, Chem. Mater. 28, 214 (2016).

- [24] A. Gupta, M. Gupta, S. Chakravarty, R. Rüffer, H.-C. Wille, and O. Leupold, Phys. Rev. B 72, 014207 (2005).
- [25] M. Gupta, A. Gupta, J. Stahn, M. Horisberger, T. Gutberlet, and P. Allenspach, Phys. Rev. B 70, 184206 (2004).
- [26] S. Dorris and M. Martin, Ber. Bunsengesellschaft Phys. Chem. 94, 721 (1990).
- [27] M. E. Fleet, Acta Crystallogr. Sect. B 37, 917 (1981).
- [28] K. Momma and F. Izumi, J. Appl. Crystallogr. **44**, 1272 (2011).
- [29] G. S. Parkinson, Surf. Sci. Rep. 71, 272 (2016).
- [30] I. S. Lyubutin, C. R. Lin, Y. V. Korzhetskiy, T. V. Dmitrieva, and R. K. Chiang, J. Appl. Phys. 106, 034311 (2009).
- [31] See Supplemental Material at <a href="http://link.aps.org/supplemental/10.1103/PhysRevLett.134.236203">http://link.aps.org/supplemental/10.1103/PhysRevLett.134.236203</a>, which includes additional Refs. [32–37], for further information about sample characterization, the point defect model and the estimation of diffusion profiles.
- [32] H. Fjellvag, F. Gronvold, S. Stolen, and B. Hauback, J. Solid State Chem. **124**, 52 (1996).
- [33] J.-E. Jørgensen, L. Mosegaard, L. E. Thomsen, T. R. Jensen, and J. C. Hanson, J. Solid State Chem. 180, 180 (2007).
- [34] E. N. Maslen, V. A. Streltsov, N. R. Streltsova, and N. Ishizawa, Acta Crystallogr. Sect. B **50**, 435 (1994).
- [35] R. Grau-Crespo, A. Y. Al-Baitai, I. Saadoune, and N. H. De Leeuw, J. Phys. Condens. Matter 22, 255401 (2010).
- [36] C. Wilkinson, A. K. Cheetham, G. J. Long, P. D. Battle, and D. A. O. Hope, Inorg. Chem. 23, 3136 (1984).
- [37] I. N. Zakharova, M. A. Shipilin, V. P. Alekseev, and A. M. Shipilin, Tech. Phys. Lett. 38, 55 (2012).
- [38] A. Stierle, T. F. Keller, H. Noei, V. Vonk, and R. Roehlsberger, J. Large-Scale Res. Facil. 2, A76 (2016).
- [39] Surfaces interfaces x-ray Scattering (SixS) beamline at the SOLEIL synchrotron, https://www.synchrotron-soleil.fr/en/beamlines/sixs (2021).
- [40] E. Vlieg, J. Appl. Crystallogr. 33, 401 (2000).
- [41] T. Pohlmann, T. Kuschel, J. Rodewald, J. Thien, K. Ruwisch, F. Bertram, E. Weschke, P. Shafer, J. Wollschläger, and K. Küpper, Phys. Rev. B 102, 220411(R) (2020).
- [42] T. N. Jensen, M. K. Rasmussen, J. Knudsen, A. Vlad, S. Volkov, E. Lundgren, A. Stierle, and J. V. Lauritsen, Phys. Chem. Chem. Phys. 17, 5795 (2015).
- [43] M. K. Rasmussen, A. S. Foster, B. Hinnemann, F. F. Canova, S. Helveg, K. Meinander, N. M. Martin, J. Knudsen, A. Vlad, E. Lundgren, A. Stierle, F. Besenbacher, and J. V. Lauritsen, Phys. Rev. Lett. 107, 036102 (2011).
- [44] G. Ketteler, W. Weiss, W. Ranke, and R. Schlogl, Phys. Chem. Chem. Phys. 3, 1114 (2001).
- [45] Y. Gao, Y. J. Kim, and S. A. Chambers, J. Mater. Res. 13, 2003 (1998).
- [46] H.-C. Wille, H. Franz, R. Röhlsberger, W. A. Caliebe, and F.-U. Dill, J. Phys. Conf. Ser. 217, 012008 (2010).
- [47] M. Andreeva, A. Smekhova, R. Baulin, Y. Repchenko, R. Bali, C. Schmitz-Antoniak, H. Wende, I. Sergueev, K. Schlage, and H.-C. Wille, J. Synchrotron Radiat. 28, 1535 (2021).
- [48] M. A. Andreeva, Hyperfine Interact. 185, 17 (2008).
- [49] M. A. Andreeva, N. G. Monina, and S. Stankov, Moscow Univ. Phys. Bull. **63**, 132 (2008).

- [50] M. Björck and G. Andersson, J. Appl. Crystallogr. 40, 1174 (2007).
- [51] M. A. Shipilin, I. N. Zakharova, A. M. Shipilin, and V. I. Bachurin, J. Surf. Invest. **8**, 557 (2014).
- [52] S. Tober, M. Creutzburg, B. Arndt, K. Krausert, S. Mattauch, A. Koutsioubas, S. Pütter, A. S. Mohd, L. Volgger, H. Hutter, H. Noei, V. Vonk, D. Lott, and A. Stierle, Phys. Rev. Res. 2, 023406 (2020).
- [53] J. Korecki, B. Handke, N. Spiridis, and T. Ślęzak, I. Flis-Kabulska, and J. Haber, Thin Solid Films **412**, 14 (2002).
- [54] R. Dieckmann, Ber. Bunsengesellschaft Phys. Chem. 86, 112 (1982).
- [55] S. Hallström, L. Höglund, and J. Ågren, Acta Mater. 59, 53 (2011).

- [56] A. Atkinson, M. L. O'dwyer, and R. I. Taylor, J. Mater. Sci. 18, 2371 (1983).
- [57] R. J. D. Tilley, *Defects in Solids* (Wiley, Hoboken, NJ, 2008).
- [58] F. Faupel, W. Frank, M.-P. Macht, H. Mehrer, V. Naundorf, K. Rätzke, H. R. Schober, S. K. Sharma, and H. Teichler, Rev. Mod. Phys. 75, 237 (2003).
- [59] E. C. Stelter and D. Lazarus, Phys. Rev. B 36, 9545 (1987).
- [60] R. Dieckmann, J. Phys. Chem. Solids 59, 507 (1998).
- [61] F. Bertram, C. Deiter, T. Schemme, S. Jentsch, and J. Wollschläger, J. Appl. Phys. 113, 184103 (2013).
- [62] V. Vonk, K. J. I. Driessen, M. Huijben, G. Rijnders, D. H. A. Blank, H. Rogalla, S. Harkema, and H. Graafsma, Phys. Rev. Lett. 99, 196106 (2007).